Journal of
Computational and Theoretical Nanoscience
Vol. 3, 1–11, 2006

A Robust Mathematical Formulation for Studying Elastically Coupled Motor-Cargo Systems

Hongyun Wang

Department of Applied Mathematics and Statistics, University of California, Santa Cruz, CA 95064, USA

Molecular motors are small, and, as a result, motor operation is dominated by high viscous friction and large thermal fluctuations from the surrounding fluid environment. The small size has made it very difficult to study the physical mechanisms of molecular motors. It is already difficult enough to see the motor itself, let alone to control the motor directly by applying an external force. In many single molecule experiments and when carrying out its biological functions, a molecular motor may be coupled elastically to a cargo that is much bigger than the motor itself. Fortunately, current experimental technologies allow us to measure the external force acting on the cargo and the position of the cargo with the precision of piconewtons and nanometers. It is not clear, however, whether the measured force and position can be simply treated as the force acting on the motor and the position of the motor itself. Thus, to interpret correctly the experimental results, we need to study the behaviors of not just the motor itself but also the elastically coupled motor-cargo systems. To facilitate the modeling study of motor-cargo systems, we must develop the corresponding numerical capability for solving the modeling equations. In this study, we develop a robust mathematical/numerical formulation for simulating elastically coupled motor-cargo systems for the full range of elasticity.

Keywords: Molecular Motors, Motor-Cargo Systems, Langevin Equations, Fokker-Planck Equations, Stokes Efficiency, Binding Zipper Model.

RESEARCH ARTICLE

1. INTRODUCTION

Molecular motors are very small and operate in a viscous fluid environment (water). Consequently, the motor motion is dominated by high viscous friction and large thermal fluctuations.[1] Because of the small size, molecular motors have several features that distinguish themselves from macroscopic motors. The most prominent feature of molecular motors is that the time scale of inertia (the time it takes for the motor to forget its current instantaneous velocity) is much smaller than the time scale of chemical reaction cycle in the motor. On the time scale of motor operation, the effect of inertia can be safely ignored. A related feature of molecular motors is that the instantaneous velocity, caused by the bombardments of surrounding fluid molecules, changes drastically over the time scale of chemical reaction cycle in the motor. The typical value of the stochastic instantaneous velocity is several orders of magnitude larger than the average velocity of the motor. In comparison, for macroscopic motors, the time scale of inertia is much larger than the time scale of reaction cycle, and the instantaneous velocity is almost constant over the time scale of reaction cycle. These peculiar features of molecular motors suggest that we have to model molecular motors as stochastic processes and take explicitly into consideration the large thermal fluctuations. In particular, results obtained for macroscopic motors should be examined carefully in the mathematical framework of stochastic processes before being applied to molecular motors. In both macroscopic motors and molecular motors, a unidirectional motion can be produced by generating an active force at the chemical reaction site and then using the active force to drive the motor forward. This mechanism of producing a unidirectional motion is called power stroke.[2, 3] In molecular motors, a unidirectional motion can also be produced by a different mechanism: if thermal fluctuations in the backward direction are blocked by a free energy barrier, then the motor will be effectively carried forward by thermal fluctuations. This mechanism of producing a unidirectional motion is called Brownian ratchet[4–8] or information ratchet.[9] In a power stroke motor, the chemical reaction generates an active driving force, which corresponds to a gradually decreasing motor potential. In a Brownian ratchet, the chemical reaction establishes a free energy barrier, which corresponds to a vertical drop followed by a flat step in the motor

*Author to whom correspondence should be addressed.

potential. These two kinds of mechanisms (power stroke and Brownian ratchet) respond differently to the externally applied conservative force and other experimental conditions. Therefore, deciphering the energy transduction mechanism in a molecular motor depends on measuring motor behaviors in response to external force and to various experimental conditions. Unfortunately, the small size of molecular motors has made it very difficult to measure directly the mechanical behaviors of the motor itself. It is not yet possible to observe/record the internal motion of a single molecule motor. Nor is it possible to observe/record the chemical occupancy state of a single molecule motor. In most single molecule experiments and when accomplishing its biological functions, a molecular motor is elastically coupled to a cargo that is much larger than the motor. The current experimental technologies allow us to measure forces acting on the cargo to the precision of piconewtons and measure position of the cargo to the precision of nanometers.[10–14] Time series of cargo positions have been measured for various elastically coupled motor-cargo systems at various mechanical loads and chemical concentrations.[15–18] From the time series of cargo positions, the average velocity and randomness parameter can be extracted.[16, 19] In the past, information extracted from cargo positions was used directly to infer the energy transduction mechanism in the motor without considering the effect of the elastic coupling between the motor and the cargo. To interpret experimental results correctly, the motor-cargo system should be studied in the mathematical framework in which the motor and the cargo evolve stochastically and are coupled elastically. To facilitate the modeling study of motor-cargo systems, we must develop the corresponding numerical capability of solving motor-cargo system. In this work, we study a robust numerical formulation for simulating elastically coupled motor-cargo systems for the full range of the linkage elasticity: from soft spring limit to the stiff spring limit. In a previous study,[20] we proposed a numerical method that can calculate all average quantities but can accommodate only the intermediate range of the linkage elasticity. Here, we propose a new robust mathematical/numerical formulation, in which, the relative motion between the motor and the cargo is separated from the motion of the motor-cargo complex. The separation of these two motions enables us to use different numerical grids for these two motions, and enables us to simulate motor-cargo systems for the full range of elasticity. This numerical capability makes it possible to compare numerical results with asymptotic results.[21, 22] Below, we will first introduce the mathematical framework for modeling the continuous motion of molecular motors and motor-cargo systems. Then we will propose a formulation that is suitable for simulating motor-cargo systems for the full range of the linkage elasticity. Finally numerical examples are shown to demonstrate the robustness of the proposed numerical formulation.

2. MATHEMATICAL FRAMEWORK FOR MODELING MOLECULAR MOTORS

In this section, we review the mathematical framework for modeling the continuous motion of molecular motors. There are many levels of modeling approaches for molecular motors: from kinetic models with a few easily observable states to all atom molecular dynamics. Models at different levels have different advantages and disadvantages. For example, a kinetic model with only a few easily observable states can be readily fitted to biochemical experimental observations but it is only a simple phenomenological model and it yields little information about the physical mechanism of the process. On the other hand, an all atom molecular dynamic simulation is almost entirely based on first principles but with today's computing facilities even for a moderately large molecule it is impossible to simulate the physical process over a time period of one millisecond, which is the time scale of chemical reaction and mechanical motion in molecular motors. Given these limitations, it seems that models of intermediate level are more practical for today's computing facilities and more promising than simple kinetic models in capturing the physical mechanism of the underlying motor.

In many chemical reactions, the mechanical motion involves only a small conformational change against no significant force, and the conformational change occurs at a time scale much smaller than that of the reaction cycle. These chemical reactions can be well described by simple kinetic models. In molecular motors, however, the mechanical motion generally involves a large conformational change against a significant conservative load and/or viscous drag, and the conformational change occurs over a time scale comparable to that of the reaction cycle. These special properties of molecular motors require that the mechanical motion be modeled explicitly as a continuous motion and be coupled to the chemical reaction. One advantage of modeling the continuous motion of molecular motors is that physical quantities of continuous motion (such as, drag force and Stokes efficiency[23]) can be directly incorporated into and discussed in the model. In general, a molecular motor has many degrees of freedom, of which there is a prominent one associated with the unidirectional motion of the motor. For example, the γ shaft of the F_0F_1 ATP synthase rotates with respect to the $\alpha_3\beta_3$ hexamer,[2, 24–27] a flagellar motor rotates the flagellar filament with respect to the cell body[28, 29] and a kinesin dimer moves along a microtubule toward the plus end.[16, 30–32] A viable modeling approach of intermediate level is to follow the motor motion explicitly only along the dimension of its unidirectional motion and to include the effects of other degrees of freedom in the mean field potential affecting the unidirectional motion.[5, 7 33, 34] Let us start by examining the one dimensional motion of a small particle in a fluid environment, subject to a potential, $V(x)$. The particle is affected by the conservative force derived from

RESEARCH ARTICLE

the potential, by the viscous drag, and by the Brownian force. The stochastic motion of the particle is governed by the Newton's second law:

$$m\frac{dv}{dt} = \underbrace{-\zeta v}_{\substack{\text{Viscous}\\ \text{drag}}} \quad \underbrace{-V'(x)}_{\substack{\text{Force from}\\ \text{potential}}} \quad \underbrace{+\sqrt{2K_BT\zeta}\frac{dW(t)}{dt}}_{\substack{\text{Brownian}\\ \text{forxe}}} \qquad (1)$$

where x is the position, v the velocity, and m the mass of the particle. $W(t)$ is the Weiner process. The viscous drag on the particle, $-\zeta v$, is always opposing the motion where ζ is called the drag coefficient. The magnitude of the Brownian force is related to the drag coefficient by $\sqrt{2K_BT\zeta}$, which is a result of the fluctuation-dissipation theorem.[35, 36] Here k_B is the Boltzmann constant, and T the absolute temperature.[37]

Because of the small size of molecular motors, motor operation is dominated by high viscous friction and thermal fluctuations from the surrounding fluid environment. In Eq. (1), the evolution of particle has two very different time scales: the very short time scale of the particle forgetting its current instantaneous velocity (the time scale of inertia) and the relatively long time scale of the particle moving along the potential. The time scale of inertia is $t_0 = m/\zeta$ or a particle of radius 0.5 μm in water, we have $t_0 \approx 56 \times 10^{-9}$ s ,[38] which is much smaller than the time scale of motor reaction cycles. If we are only concerned with evolution over time scales much larger than t_0, then we can safely ignore the effect of inertia. Ignoring the effect of inertia eliminates the time scale of inertia from Eq. (1) and reduces Eq. (1) to a Langevin equation that is no longer stiff:

$$\frac{dx}{dt} = -D\frac{V'(x)}{k_BT} + \sqrt{2D}\frac{\mathrm{d}W(t)}{dt} \qquad (2)$$

where $D = k_BT/\zeta$ is the diffusion coefficient.[1] To illustrate intuitively the reduction from Eq. (1) to Eq. (2), we rewrite Eq. (1) as

$$\frac{dv}{dt} = \frac{-1}{t_0}\left[v - \left(-D\frac{V'(x)}{k_BT} + \sqrt{2D}\frac{dW(t)}{dt}\right)\right], \quad t_0 = \frac{m}{\zeta} \qquad (3)$$

Formally, Eq. (3) is similar to the simple model equation below

$$\frac{dv}{dt} = \frac{-1}{t_0}[v - f(v)]$$

The exact solution of the model equation is given by

$$v(t) = f(t) + \exp\left(\frac{-t}{t_0}\right)(y(0) - f(0)) + \frac{1}{t_0}\int_0^t \exp\left(\frac{-(t-s)}{t_0}\right)(f(s) - f(t))\,ds$$

For $t_0 \ll 1$ and $t \gg t_0$, expanding the integral in the exact solution yields

$$v(t) = f(t) - f'(t)t_0 + O(t_0^2) + \exp\left(\frac{-t}{t_0}\right)(y(0) - f(0))$$

Thus, we have approximately $v(t) = f(t)$. Applying this result to Eq. (3) yields

$$v(t) = \left(-D\frac{V'(x)}{k_BT} + \sqrt{2D}\frac{dW(t)}{dt}\right)$$

which leads directly to Eq. (2). Eq. (2) is the Langevin equation without inertia governing the stochastic motion of a small particle driven by potential $V(x)$. In a molecular motor, the motion is driven by switching among a set of periodic potentials $\{\phi_S(x)\}$, each corresponding to a chemical occupancy state (S) of the motor. Suppose the chemical reaction cycle has N occupancy states. Then the motor motion is governed by a set of Langevin equations of the form (2) with potential replaced by $\{\phi_S(x),\ S = 1, 2, \ldots, N\}$. At any given time, the motor motion is governed by one Langevin equation in the set, corresponding to the current chemical state of the motor.[5, 33] As the chemical reaction proceeds, the current chemical state jumps to a different state and the motor motion is governed by a different Langevin equation in the set, corresponding to the new chemical state of the motor.

For ATPase motors, each catalytic site has four occupancy states:[24, 39–41]

$$\begin{array}{ccc} [\mathbf{SITE}] + \ldots & \Longleftrightarrow & [\mathbf{SITE} * \mathrm{ATP}] \\ \Updownarrow & & \Updownarrow \\ [\mathbf{SITE} * \mathrm{ADP}] + \ldots & \Longleftrightarrow & [\mathbf{SITE} * \mathrm{ADP} * P_i] \end{array}$$

The F_1-ATP synthase has three catalytic sites so it has $N = 4 \times 4 \times 4 = 64$ occupancy states. We use a continuous time discrete space Markov process (a jump process) to model the stochastic evolution of the chemical occupancy state. The jump process is completely specified by the transition rates $\{k_{j\to i}(x)\}$. In the mathematical form, all transition rates are contained in the transition matrix $\mathbf{K}(x) = \{k_{i,j}(x)\}$. For $j \neq i$, $k_{i,j}(x) = k_{j\to i}(x)$ is the transition rate from state j to state i. The diagonal elements of the transition matrix are defined as: $k_{i,j}(x) = -\Sigma_{i\neq j}k_{j\to i}(x)$. Thus, the transition matrix always satisfies $\Sigma_i k_{ij}(x) = 0$. This property will be used later when we discuss the motor potential profile. In molecular motors, the chemical reaction is generally coordinated by the motor position. Consequently the transition matrix is a function of motor position.

Instead of following the stochastic evolution (mechanical motion and chemical transition) of an individual motor, we can follow the deterministic evolution of probability density. The advantage of following the probability density is that (a) it can be solved numerically with high accuracy and (2) all experimentally observable quantities can be calculated from the probability density. Let us consider an ensemble of motors, each evolving in time independently and stochastically. Let $\rho_S(x, t)$ be the probability density that the motor is at position x and in occupancy state S at time t. The time evolution of $\rho_S(x, t)$ is governed by the

Fokker-Planck Equation:[42, 43]

$$\frac{\partial \rho_S}{\partial t} = D\frac{\partial}{\partial x}\left(\underbrace{\frac{\phi_S'(x)}{k_BT}\rho_S}_{\text{Convection}} + \underbrace{\frac{\partial \rho_S}{\partial x}}_{\text{Diffusion}}\right) + \underbrace{\sum_{j=1}^{N} k_{Sj}(x)\rho_j}_{\text{Change of occupancy}}$$

$$S = 1, 2, \ldots, N \tag{4}$$

Equation (4) is a mathematical framework for modeling the continuous motion of molecular motors.[8, 23, 33, 44–47] In Eq. (4), $\phi_S(x)$'s are periodic with period L, where the period L is usually a multiple of motor steps. A hypothetical motor driven by switching among a set of 3 potentials is illustrated in Figure 1.

In modeling studies using mathematical framework (4), experimental measurements and structural information may be used to infer the set of N potentials driving the motor. Usually we will not have enough information to determine all N potentials. In this sense, current modeling studies still depend on our imagination in constructing the full set of N potentials. It is desirable if the motor operation can be characterized by one potential. Let us consider the steady state of Eq. (4). Summing over S, we have

$$0 = D\frac{\partial}{\partial x}\left(\frac{\psi'(x)}{k_BT}\rho + \frac{\partial \rho}{\partial x}\right) \tag{5}$$

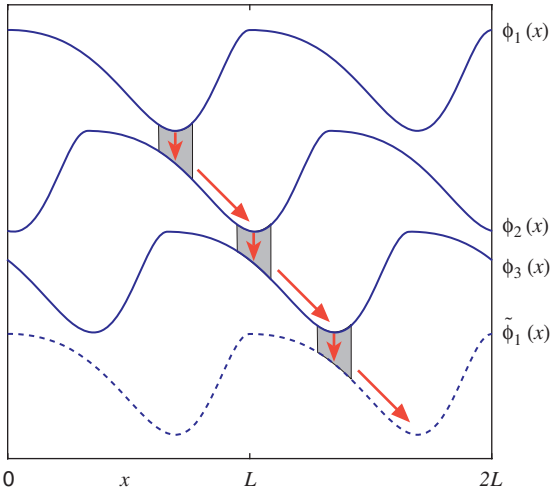

Fig. 1. A motor system driven by switching among a set of three potentials $\{\phi_S(x),\ S = 1,\ 2,\ 3\}$. Two periods of potentials are shown. In one reaction cycle, the motor start at the minimum of potential $\phi_1(x)$. The shaded region indicates where the chemical transition can occur. After switching to potential $\phi_2(x)$, the motor is driven by potential $\phi_2(x)$ to the minimum of $\phi_2(x)$ where the motor is allowed to switch to potential $\phi_3(x)$. Sliding to the minimum of potential $\phi_3(x)$ and switching to $\tilde{\phi}_1(x)$, the motor arrives at the minimum of $\tilde{\phi}_1(x)$ at the end of one reaction cycle. In one reaction cycle, the motor moves forward by a distance of L. Notice that $\tilde{\phi}_1(x)$ is the same as $\phi_1(x)$ except that it is shifted downward in the direction of free energy by ΔG (free energy change of one reaction cycle). From the point of view of energetics, $\phi_1(x)$ is the starting point of the current cycle and $\tilde{\phi}_1(x)$ is the end point of the current cycle and the starting point of the next cycle. In the mathematical formulation, we only keep track of the occupancy state so we group $\tilde{\phi}_1(x)$ and $\phi_1(x)$ together.

where $\rho(x) = \sum_{i=1}^{N} \rho_i(x)$ is the steady state probability density regardless of the chemical state. In the above we have used the property $\sum_{i=1}^{N} k_{i,j}(x) = 0$ so that the chemical reaction terms disappear in the sum. The motor potential profile, $\psi(x)$, is defined as

$$\psi'(x) = \frac{l}{\rho(x)}\sum_{i=1}^{N} \phi_i'(x)\,\rho_i(x) \tag{6}$$

In Eq. (5), the steady state probability density $\rho(x)$ behaves as if the motor were driven by a single potential $\psi(x)$. In this sense, the motor potential profile $\psi(x)$ represents the overall effect of the chemical reaction on the motor motion. Because $\{\phi_S(x),\ S = 1,\ 2,\ \ldots,\ N\}$ are periodic with period L, $\psi'(x)$ is periodic and $\psi(x)$ is a tilted periodic function. The potential profile $\psi(x)$ can be written as $\psi(x) = \phi(x) - \Delta\psi x/L$ where $\phi(x)$ is periodic with period L and $\Delta\psi = \psi(0) - \psi(L)$ can be viewed as the potential energy made available in the chemical reaction per displacement L for driving the motor motion. This suggests a simplified mathematical framework for modeling molecular motors: the motor operation can be characterized by a tilted periodic potential.

3. A ROBUST MATHEMATICAL FORMULATION FOR SIMULATING MOTOR-CARGO SYSTEMS

In many single molecule experiments[15, 16, 18, 48] and when carrying out its biological functions, a molecular motor is elastically linked to a cargo that is much bigger than the motor itself. The conservative force exerting on the cargo can be controlled to a precision of piconewton and time series of cargo positions can be observed and recorded with a precision of nanometer. Two motor-cargo systems are shown in Figure 2. Figure 2(A) shows the experimental setup in Ref. [15] where the $\alpha_3\beta_3$ hexamer of the F_1-ATP synthase is attached to the cover glass and a long actin filament (0.5 μm ~2 μm) is attached to the γ shaft to visualize the rotation of the γ shaft. When ATP is added the γ shaft rotates counter-clockwise. The γ shaft has torsional elasticity so the motor and the cargo (actin filament) are actually elastically coupled. Figure 2(B) shows the experimental setup in Refs. [11] and [16] where a kinesin dimer walks on a microtubule toward the plus end and a latex bead is linked to the kinesin dimer to visualize the motion of the kinesin dimer and to exert a force on the kinesin dimer. Since the linkage between the kinesin dimer (motor) and the latex bead (cargo) is elastic, the motor and the cargo are elastically coupled. In Figure 2(B), the force exerting on the kinesin dimer is controlled either by changing the size of the latex bead and changing the viscosity of the surrounding fluid[11] or by applying a force on the bead using a laser trap.[16] In the recently developed 2-D laser trap,[18] a force perpendicular to the direction of motor motion can also be exerted on the kinesin dimer.

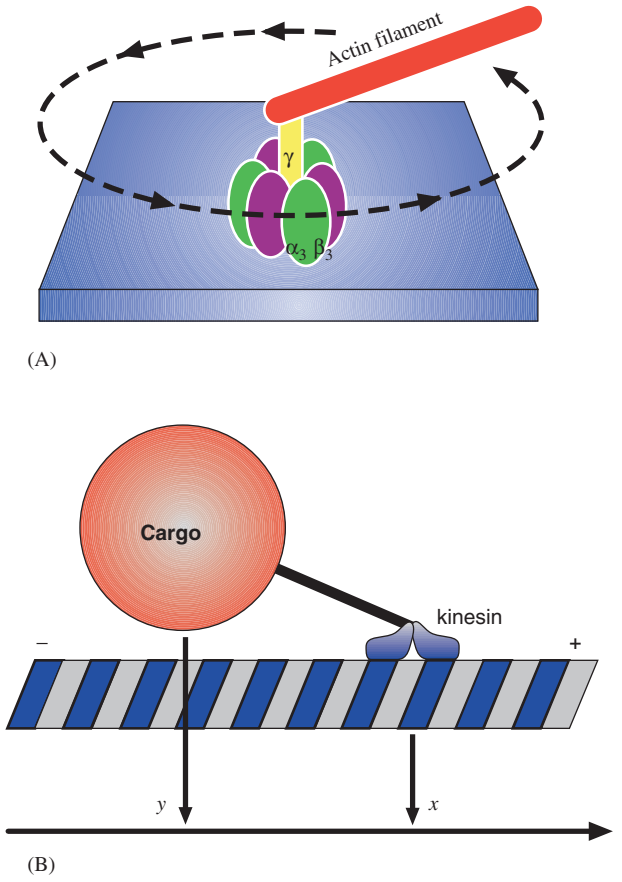

Fig. 2. Two motor-cargo systems in single molecule experiments. (A) The experimental setup in Ref. [15]: the $\alpha_3\beta_3$ hexamer of the F_1-ATP synthase is attached to the cover glass and a long actin filament (0.5 μm ~2 μm) is attached to the γ shaft to visualize the rotation of the γ shaft. (B) The experimental setup in Refs. [11] and [16]: a kinesin dimer walks on microtubule toward the plus end and a latex bead is linked to the kinesin dimer to visualize the motion of the kinesin dimer and to exert a force on the kinesin dimer.

Let x be the coordinate of the motor and y the coordinate of the cargo along the direction of motion as illustrated in Figure 2(B). If the motor is modeled as being driven by a set of N periodic potentials as in Eq. (4), then the motor-cargo system is governed by Fokker-Planck equation

$$\begin{aligned}
&\frac{\partial \rho_S}{\partial t} = -\frac{\partial}{\partial x} J_S(x,y) - \frac{\partial}{\partial y} I_S(x,y) + \sum_{j=1}^{N} k_{Sj}(x)\,\rho_j, \\
&\qquad S = 1, 2, \ldots, N \\
&J_S(x,y) = -D_M\left(\frac{1}{k_B T}\frac{\partial \Phi_S(x,y)}{\partial x}\rho_S + \frac{\partial \rho_S}{\partial x}\right), \\
&\qquad S = 1, 2, \ldots, N \\
&I_S(x,y) = -D_C\left(\frac{1}{K_B T}\frac{\partial \Phi_S(x,y)}{\partial y}\rho_S + \frac{\partial \rho_S}{\partial y}\right) \\
&\qquad S = 1, 2, \ldots, N \\
&\Phi_S(x,y) = \phi_S(x) + \frac{\kappa}{2}(x-y-R)^2, \\
&\qquad S = 1, 2, \ldots, N
\end{aligned} \tag{7}$$

where $J_S(x,y)$ and $I_S(x,y)$ are respectively, the probability flux in the x-dimension and the y-dimension in chemical occupancy state S. D_M is the diffusion coefficient of the motor and D_C the diffusion coefficient of the cargo. $\Phi_S(x,y)$ is the total potential energy of the motor-cargo system in chemical occupancy state S. $\Phi_S(x,y)$ includes both the motor internal potential energy caused by the chemical reaction and the elastic energy in the link connecting the motor and the cargo. In the above, κ is the elasticity of the link and R is the rest length of the elastic link. The rest length R can be eliminated using a change of variable $\bar{y} = y + R$. So without loss of generality, we assume $R = 0$.

If the motor is modeled as being driven by a tilted periodic potential as in Eq. (5), then the Fokker-Planck equation for the motor-cargo system is

$$\begin{aligned}
\frac{\partial \rho}{\partial t} &= D_M \frac{\partial}{\partial x}\left(\frac{1}{k_B T}\frac{\partial \Psi(x,y)}{\partial x}\rho + \frac{\partial \rho}{\partial x}\right) \\
&\quad + D_C \frac{\partial}{\partial y}\left(\frac{1}{k_B T}\frac{\partial \Psi(x,y)}{\partial y}\rho + \frac{\partial \rho}{\partial y}\right) \qquad (8) \\
\Psi(x,y) &= \psi(x) + \frac{\kappa}{2}(x-y)^2
\end{aligned}$$

For simplicity, we focus our discussion on the Fokker-Planck equation without reaction (8). The mathematical formulation derived and numerical method developed for (8) can be easily extended to the Fokker-Planck equation with reaction (7). Equation (8) in its current form has two disadvantages for numerical computations. (1) In the stiff spring limit the cargo follows the motor very closely and any slight separation of the cargo from the motor is penalized by a large increase in the elastic energy $0.5\,\kappa(x-y)$.[2] In a straightforward numerical formulation based directly on Eq. (8), however, the system moves in the x-dimension and in the y-dimension separately. In particular, the system cannot move directly from grid point $(\Delta x, \Delta y)$ to grid point $(2\Delta x, 2\Delta y)$ without having to go through $(\Delta x, 2\Delta y)$, or $(2\Delta x, \Delta y)$. In the stiff spring limit, going through $(\Delta x, 2\Delta y)$ or $(2\Delta x, \Delta y)$ involves a large increase in elastic energy $0.5\,\kappa(x-y)^2$ unless the grid size is extremely small. (2) As the motor moves forward the cargo has to more or less follow the motor so the computational domain in the y-dimension changes with x. In particular, if the period of the motor potential is L, then the computational domain for y at $x = L$ is the computational domain for y at $x = 0$ shifted up by L. In numerical methods, to implement the periodic boundary condition in the x-dimension, we need to connect the grid points for y at $x = L$ to the grid points at $x = 0$, which requires that L be an integer multiple of the step size in the y-dimension. This certainly restricts how we draw numerical grid in the y-dimension and affects our ability of dealing with the soft spring limit where the computational domain for y may be very large and it may be difficult to enforce that L is an integer multiple of the step size in the y-dimension.

RESEARCH ARTICLE

To overcome these two difficulties, we write Eq. (8) in a different form. The goal is to separate the degree of freedom associated with the relative motion between the motor and the cargo from that associated with the motion of the motor-cargo complex. After these two degrees of freedom are separated, we can use very different computational domain and very different step size to treat the relative motion between the motor and the cargo. That will allow us to handle the full range of elasticity efficiently. To achieve the goal, we start by scaling x and y to make D_M and D_C disappear so after scaling both dimensions have diffusion coefficients equal to 1. Consider the scaling

$$\begin{cases} \tilde{x} = \dfrac{1}{\sqrt{D_M}} x \\ \tilde{y} = \dfrac{1}{\sqrt{D_C}} y \end{cases}, \qquad \begin{cases} x = \sqrt{D_M}\,\tilde{x} \\ y = \sqrt{D_C}\,\tilde{y} \end{cases}$$

Under this scaling, Eq. (8) becomes

$$\begin{aligned} \frac{\partial \tilde{\rho}}{\partial t} &= \frac{\partial}{\partial \tilde{x}}\left(\frac{1}{k_B T}\frac{\partial \tilde{\Psi}(\tilde{x},\tilde{y})}{\partial \tilde{x}}\tilde{\rho} + \frac{\partial \tilde{\rho}}{\partial \tilde{x}}\right) \\ &\quad + \frac{\partial}{\partial \tilde{y}}\left(\frac{1}{k_B T}\frac{\partial \tilde{\Psi}(\tilde{x},\tilde{y})}{\partial \tilde{y}}\tilde{\rho} + \frac{\partial \tilde{\rho}}{\partial \tilde{y}}\right) \qquad (9) \\ \tilde{\rho}(\tilde{x},\tilde{y},t) &= \sqrt{D_M D_C}\,\rho\left(\sqrt{D_M}\tilde{x}, \sqrt{D_C}\tilde{y}, t\right) \\ \tilde{\Psi}(\tilde{x},\tilde{y}) &= \psi(\sqrt{D_M}\tilde{x}) + \frac{\kappa}{2}\left(\sqrt{D_M}\tilde{x} - \sqrt{D_C}\tilde{y}\right)^2 \end{aligned}$$

where the factor in front of $\rho(x, y, t)$ is to make it integrate to one. Next we rotate the coordinate system in the $\tilde{x}\tilde{y}$-plane to make $\sqrt{D_M}\tilde{x} - \sqrt{D_C}\tilde{y}$ an independent variable. Since both the $\tilde{x}$-dimension and the $\tilde{y}$-dimension have the same diffusion coefficient, an orthogonal transformation will not create any mixed second derivative. Consider the orthogonal transformation

$$\begin{cases} \xi = \dfrac{1}{\sqrt{D_C + D_M}}\left(\sqrt{D_C}\,\tilde{x} + \sqrt{D_M}\,\tilde{y}\right) \\ \eta = \dfrac{1}{\sqrt{D_C + D_M}}\left(-\sqrt{D_M}\,\tilde{x} + \sqrt{D_C}\,\tilde{y}\right) \end{cases}$$

Expressing $(\tilde{x}, \tilde{y})$ in terms of, we get

$$\begin{cases} \tilde{x} = \dfrac{1}{\sqrt{D_C + D_M}}\left(\sqrt{D_C}\,\xi - \sqrt{D_M}\,\eta\right) \\ \tilde{y} = \dfrac{1}{\sqrt{D_C + D_M}}\left(\sqrt{D_M}\,\xi + \sqrt{D_C}\,\eta\right) \end{cases}$$

After the orthogonal transformation, Eq. (9) becomes

$$\begin{aligned} \frac{\partial \rho}{\partial t} &= \frac{\partial}{\partial \xi}\left(\frac{1}{k_B T}\frac{\partial V(\xi,n)}{\partial \xi}\rho + \frac{\partial \rho}{\partial \xi}\right) \\ &\quad + \frac{\partial}{\partial \eta}\left(\frac{1}{k_B T}\frac{\partial V(\xi,\eta)}{\partial \eta}\rho + \frac{\partial \rho}{\partial \eta}\right) \end{aligned}$$

$$\begin{aligned} \rho(\xi,\eta,t) &= \sqrt{D_C D_M}\,\rho\left(\frac{\sqrt{D_M}}{\sqrt{D_C + D_M}}\left(\sqrt{D_C}\xi - \sqrt{D_M}\eta\right),\right. \\ &\quad \left. \times \frac{\sqrt{D_C}}{\sqrt{D_C + D_M}}\left(\sqrt{D_M}\xi + \sqrt{D_C}\eta\right), t\right) \\ V(\xi,\eta) &= \psi\left(\frac{\sqrt{D_M}}{\sqrt{D_C + D_M}}\left(\sqrt{D_C}\xi - \sqrt{D_M}\eta\right)\right) \\ &\quad + \frac{\kappa}{2}(D_C + D_M)\eta^2 \qquad (10) \end{aligned}$$

In Eq. (10), the total potential $V(\xi, \eta)$ is periodic in the ξ-dimension with period $L_\xi = L(\sqrt{D_C + D_M}/\sqrt{D_C D_M})$. In the η-dimension, as $\to \pm\infty$, potential $V(\xi, \eta)$ is dominated by the elastic potential $\kappa/2(D_C + D_M)\eta^2$. It is important to point out that Eqs. (8) and (10) are the mathematical governing equations in different coordinates for the same underlying physical system (a elastically coupled motor-cargo system). Mathematically they are equivalent to each other. In particular, Eqs. (8) and (10) will yield the same average velocity and effective diffusion. From computational point of view, Eq. (10) is more convenient than Eq. (8) in several aspects. First, the distance between the motor and the cargo is now isolated in coordinate η. The elastic energy is a function of η only and is independent of ξ. Eq. (10) is periodic in ξ with period L_ξ. This allows us to use a computational domain of size L_ξ for the ξ-dimension and apply a periodic boundary condition in computation. In the η-dimension, the computational domain is no longer affected by the ξ coordinate so a suitable numerical grid can be selected for the η-dimension without having to move it up and down to accommodate the ξ coordinate. More important, now it is possible to use a numerical grid for the η-dimension that is tailored to the stiffness of the elastic link between the motor and the cargo. For example, for stiff linkage, the motor and the cargo are constrained to a small neighborhood of each other, and the elastic energy is very sensitive to the relative displacement between the motor and the cargo. Thus, for a stiff linkage, we use a small computational domain and small grid size for the η-dimension. When the linkage is soft, the distance between the motor and the cargo is only loosely constrained by the elastic energy when they get too far away from each other. Thus, for a soft linkage, we use a large computational domain for the η-dimension. In this way, we are able to accommodate the full range of the elasticity: from the stiff spring limit to the soft spring limit. Equation (10) is the mathematical formulation we will use with the numerical method[49] to simulate the behavior of elastically linked motor-cargo systems.

4. THE NUMERICAL METHOD

In this section, we describe a numerical method for solving the Fokker-Planck Eq. (10). For the convenience of presentation and discussion, we write Eq. (10) into a conservation

form, replace (ξ, η) by (x, y) to denote independent variables, and replace L_ξ by L to denote the period.

$$\begin{aligned} \tfrac{\partial \rho}{\partial t} &= -\frac{\partial}{\partial x} J(x,y) - \frac{\partial}{\partial y} I(x,x) \\ J(x,y) &= -\left(\frac{\partial V(x,y)}{\partial x}\rho + \frac{\partial \rho}{\partial x}\right) \\ I(x,y) &= -\left(\frac{\partial V(x,y)}{\partial y}\rho + \frac{\partial \rho}{\partial y}\right) \end{aligned} \tag{11}$$

where the total potential $V(x, y)$ satisfies

$$\begin{aligned} V(x+L,y) &= V(x,y) \\ \frac{V(x,y)}{y^2} &\to c > 0 \quad \text{as} \quad |y| \to \infty \end{aligned}$$

Notice that we have normalized the potential by $k_B T$. In Eq. (11), (x, y) does not represent the positions of motor and cargo in Eq. (8). Instead, (x, y) in Eq. (11) corresponds to (ξ, η) in Eq. (10). Similarly, the period L in Eq. (11) corresponds to the period L_ξ in Eq. (10), not the period L in Eq. (8).

To discretize Eq. (11) in spatial dimensions, we start by dividing $[0, L]$ in the x-dimension into M_x subintervals of the size $h_y = L/M_x$. In the y-dimension, we select a suitable computational domain $[a, b]$ based on the dependence of $V(x, y)$ on y, and divide it into M_y subintervals of the size $h_y = (b-a)/M_y$. The numerical grid is formed as

$$\begin{aligned} h_x &= \frac{L}{M_x}, \quad x_i = \frac{-1}{2}h_x + ih_x \\ x_{i+1/2} &= \frac{-1}{2}h_x + \left(i+\frac{1}{2}\right)h_x \\ h_y &= \frac{(b-a)}{M_y}, \quad y_j = a + \frac{-1}{2}h_y + jh_y \\ y_{j+1/2} &= a + \frac{-1}{2}h_y + \left(j+\frac{1}{2}\right)h_y \end{aligned}$$

The rectangle $[x_{i-1/2}, x_{i+1/2}] \times [y_{j-1/2}, y_{j+1/2}]$ is called a cell and is represented by its center (x_i, y_j), which is the grid point (i, j). Each cell center (i, j) is also called a site. In Ref. [49], a robust numerical method was developed for solving Fokker-Planck equations. Below this method will be referred to as the WPE method. A Fokker-Planck equation governs the probability density for a continuous time and continuous space Markov process (a Langevin equation). The philosophy of the WPE method is that the Langevin equation is approximated by a continuous time and discrete space Markov process (a jump process) and the Fokker-Planck equation is approximated by the master equation of the jump process. In the jump process, the system is restricted to reside on a set of discrete sites $\{(i, j)\}$ and is only allowed to jump to an adjacent site in a single jump. The numerical grid and the jump process are illustrated in Figure 3. The key step in the discretization is to approximate the probability flux across the border separating two adjacent cells.

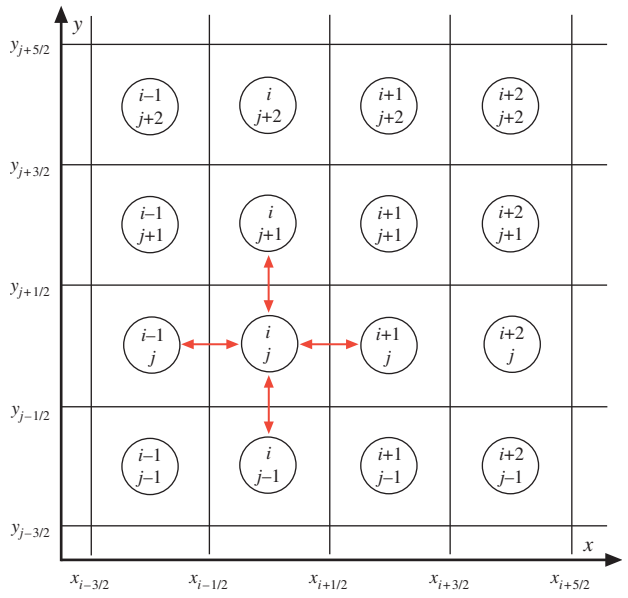

Fig. 3. Numerical grid and spatial discretization of Fokker-Planck Eq. (11). Both the x-dimension and the y-dimension are divided into small intervals, and the two dimensional region is divided into small rectangular regions. Each rectangular region is called a cell and is represented by its center (i, j). Each cell center (i, j) is also called a site. In the spatial discretization, the underlying stochastic process of Eq. (11) is approximated by a jump process where the system is restricted to residing on a set of discrete sites $\{(i, j)\}$ and is only allowed to jump to an adjacent site in a single jump.

Let $p_{i,j}(t)$ be the probability that the system is at site (i, j) at time t in the jump process. Since the site (i, j) represents the cell (i, j), $p_{i,j}(t)$ can be viewed as

$$p_{i,j}(t) = \int_{\text{cell}(i,j)} \rho(x,y)\,dxdy = h_x h_y \rho(x_i, y_j, t)$$

Let $J^{(j)}_{i+1/2}$ be the numerical probability flux in the horizontal direction, to the right, through the border separating cells (i, j) and $(i+1, j)$. Let $I^{(i)}_{j+1/2}$ be the numerical probability flux in the vertical direction, upward, through the border separating cells (i, j) and $(i, j+1)$. In the numerical method, $p_{i,j}(t)$ is governed by conservation of probability.

$$\frac{d}{dt}p_{i,j} = J^{(j)}_{i-1/2} - J^{(j)}_{i+1/2} + I^{(i)}_{J-1/2} - I^{(i)}_{j+1/2} \tag{12}$$

In the WPE method,[49] numerical fluxes $J^{(j)}_{i+1/2}$ and $I^{(i)}_{j+1/2}$ are calculated using local steady state solutions and are given by

$$\begin{aligned} J^{(j)}_{i+1/2} &= \frac{1}{(h_x)^2}\frac{\delta V^{(x,j)}_{i+1/2}}{\exp(\delta V^{(x,j)}_{i+1/2}) - 1}\left(p_{i,j} - p_{i+l,j}\exp(\delta V^{(x,j)}_{i+1/2})\right) \\ I^{(i)}_{j+1/2} &= \frac{1}{(h_y)^2}\frac{\delta V^{(y,i)}_{i+1/2}}{\exp(\delta V^{(y,i)}_{j+1/2}) - 1}\left(p_{i,j} - p_{i,j+l}\exp(\delta V^{(y,j)}_{j+1/2})\right) \end{aligned} \tag{13}$$

RESEARCH ARTICLE

where

$$\delta V^{(x,j)}_{i+1/2} = V(x_{i+1}, y_j) - V(x_i, y_j)$$
$$\delta V^{(y,i)}_{j+1/2} = V(x_i, y_{j+1}) - V(x_i, y_j)$$

Recently we proposed an improved version of the WPE method,[50] in which numerical fluxes $J^{(j)}_{i+1/2}$ and $I^{(i)}_{j+1/2}$ are given by

$$J^{(j)}_{i+1/2} = \frac{1}{(h_x)^2} \cdot \frac{2}{\exp(\delta V^{(x,j)}_{i+1/2})+1} (p_{i,j} - p_{i+1,j}\exp(\delta V^{(x,j)}_{i+1/2})) \tag{14}$$

$$I^{(i)}_{j+1/2} = \frac{1}{(h_y)^2} \cdot \frac{2}{\exp(\delta V^{(y,i)}_{j+1/2})+1} (p_{i,j} - p_{i,j+1}\exp(\delta V^{(y,i)}_{j+1/2}))$$

The improved WPE method has the advantage that there is no numerical singularity in the probability fluxes given in (14). In comparison, the probability fluxes of the WPE method given in (13) have a numerical singularity when δV approaches zero. When δV is very small, a straightforward numerical evaluation of the probability fluxes based on (13) will suffer from numerical cancellation. As a result, when δV is very small, the probability fluxes of the WPE method are calculated using an alternative formula obtained by expanding (13). In the improved WPE method (14), however, all probability fluxes are calculated using one formula. This simplifies the implementation of the improved WPE method[50] and makes it easy to port the method to a parallel computing environment.

Since everything is periodic in the x-dimension, the computational domain for the x-dimension is simply one period and the periodic boundary condition is applied:

$$V(x_{M_x+1}, y_j) = V(x_1, y_j), \quad P_{M_x+1,j} = P_{l,j},$$
$$J^{(j)}_{M_x+1/2} = J^{(j)}_{1/2}$$

The computational domain in the y-dimension, unfortunately, is not naturally bounded. But since $V(x, y)$ is asymptotically a positive quadratic form for large y, the probability density decays as

$$\rho(x, y) \sim \exp(-cy^2) \quad |y| \to \infty$$

Thus, for any given error tolerance, we can find an interval (a, b) that is large enough to include all probability with the given error tolerance. We use such an interval (a, b) as the computational domain for the y-dimension. To conserve the total probability, we place artificial reflecting boundaries at the two end of the interval. More specifically, in the numerical method, we set

$$I^{(i)}_{1/2} = 0 \quad I^{(i)}_{M_y+1/2} = 0$$

Note that the computational domain for the y-dimension should be selected large enough such that the probability of reaching the boundary cells is small. The time integration of (12) can be carried out using the Crank-Nicolson method (trapezoidal method) or an implicit Runge-Kutta that is L-stable. Most experimentally observable quantities (including average velocity and effective diffusion) can be calculated from steady state solutions of (12) and other related equations. To solve for the steady state solution of (12), we do not have to follow the time evolution of (12). Instead, the steady state solution of (12) can be obtained directly by solving a linear system consisting of the right hand side of (12) and the constraint $\Sigma_{i,j} P_{i,j} = 1$.

5. NUMERICAL EXAMPLE AND DISCUSSIONS

To test the numerical method described in the previous section, we consider a motor-cargo system where the motor is driven by a tilted periodic potential. More specifically, the motor is driven by a ratchet mechanism. The ratchet step size is $L = 2\pi/3 = 120°$. The free energy barrier of the ratchet is $\Delta G = 20\ k_B T$, corresponding to the free energy change of one ATP hydrolysis cycle. Mathematically, the tilted periodic potential is given by

$$\psi(x) = \phi(x) - \Delta G \frac{x}{L} \tag{15}$$
$$\phi(x) = \Delta G \frac{x}{L} \quad \text{for} \quad 0 < x < L, \quad \phi(x+L) = \phi(x)$$

This example can be viewed as a simple model for the motor-cargo system consisting of the F_1 ATPase and a long actin filament illustrated in Figure 2(A). Indeed it is a model problem for studying the energy transduction of the F_1 ATPase. The diffusion coefficient of the cargo is $D_C = 4$ rad^2/s, corresponding to the rotational diffusion coefficient of an actin filament of 1 μm in length around its end, and the diffusion coefficient of the motor (the lower portion of the γ shaft rotating inside the $\alpha_3\beta_3$ hexamer) is taken as $D_M = 4 \times 10^5$ rad^2/s. The motor is represented by the lower portion of the γ shaft and the cargo is the long actin filament. The link between the motor and the cargo is the upper portion of the γ shaft. The torsional elasticity κ, of the link is estimated by modeling the upper portion of the γ shaft as a homogeneous elastic rod and using Young's longitudinal module of actin[51]

$$\kappa = \frac{\pi R^4 E}{4l(1+\sigma)} = 100 \text{ PN} \cdot \text{nm/rad}^2$$

where $R = 0.8$ nm is the radius of the γ shaft, $l = 4$ nm is the length of the upper portion of the γ shaft that couples the F_1 motor to the actin filament, $\sigma = 0.4$ is the Poisson ratio, and $E = 1.8 \times 10^3$ pN nm^{-2} is Young's longitudinal modulus for an actin filament. The assumption that the γ shaft be a homogeneous rod is supported by the fact that the same assumption has been shown to be valid for actin filaments. The torsional rigidity of single actin filaments has been determined experimentally.[52] The experimentally determined value agrees well with the theoretical value predicted from the longitudinal rigidity under the assumption that the actin filament is a homogeneous rod.[52] The goal of the model problem is to see whether or not

the estimated torsional elasticity of the link along with the large diffusion coefficient of the γ shaft is capable of smoothing out the ratchet potential and producing the high Stokes efficiency of the F_1 ATPase observed in experiments.[15] The Stokes efficiency of the motor-cargo system is defined as[23]

$$\eta_{\text{Stokes}} = \frac{(\zeta_C + \zeta_M)\langle v\rangle L}{\Delta G}$$

where $\zeta_M = k_B T/D_M$ is the drag coefficient of the motor, $\zeta_C = k_B T/D_C$ the drag coefficient of the cargo, and $\langle v\rangle$ the average velocity. The Stokes efficiency can be written as

$$\eta_{\text{Stokes}} = \frac{\langle v\rangle}{\frac{\Delta G/L}{(\zeta_C+\zeta_M)}} \tag{16}$$

In (16), the numerator is the actual average velocity of the motor-cargo system while the denominator $\Delta G/L/(\zeta_C + \zeta_M)$ is the velocity that would be achieved if the free energy ΔG is utilized uniformly over a displacement of L to produce a constant force $\Delta G/L$ to drive the motor-cargo complex. When the cargo is much larger than the motor, we have $\zeta_C + \zeta_M = \zeta_C$. In the simple model we consider here, at the stiff spring limit, the motor-cargo system is simply one object driven by the tilted periodic potential (15). When the cargo is much larger than the motor, the diffusion coefficient of the motor-cargo complex is

$$D = \frac{D_C D_M}{D_C + D_M} = D_C$$

The Stokes efficiency of a motor driven by a tilted periodic potential is given by:[23]

$$\eta_{\text{Stokes}} = \frac{\int_0^L \exp\left(-\frac{\Delta G}{k_B T}\frac{s}{L}\right) ds}{\int_0^L \underbrace{\frac{1}{L}\int_0^L \exp\left[\frac{(\phi(s+x)-\phi(x))}{k_B T}\right] dx}_{\text{Effect of } \phi \text{ on efficiency}} \exp\left(\frac{-\Delta G}{k_B T}\frac{s}{L}\right) ds}$$

where the term containing the effect of $\phi(x)$ on the Stokes efficiency satisfies

$$E[\phi] \equiv \frac{1}{L}\int_0^L \exp\left[\frac{(\phi(s+x)-\phi(x))}{k_B T}\right] dx \geq 1$$

So the Stokes efficiency is always bounded by 100%. When $\psi(x)$ is close to a constant slope, $\phi(x)$ is close to zero and $E[\phi] \approx 1$. In this case, the Stokes efficiency is close to 100%. When $\psi(x)$ deviates from a constant slope, the Stokes efficiency decreases. For the ratchet potential given in (15), the Stokes efficiency is $\eta_{\text{Stokes}} \approx 10\%$. Therefore, at the stiff spring limit, the Stokes efficiency of the motor-cargo system is $\eta_{\text{Stokes}} \approx 10\%$. In general, the elasticity in the link helps to smooth out the unevenness in the driving force of the motor and helps to achieve a higher Stokes efficiency for the motor-cargo system.

In this study we mainly use this simple model to test the robustness of the numerical method. For that purpose, we carry out simulations using the numerical method

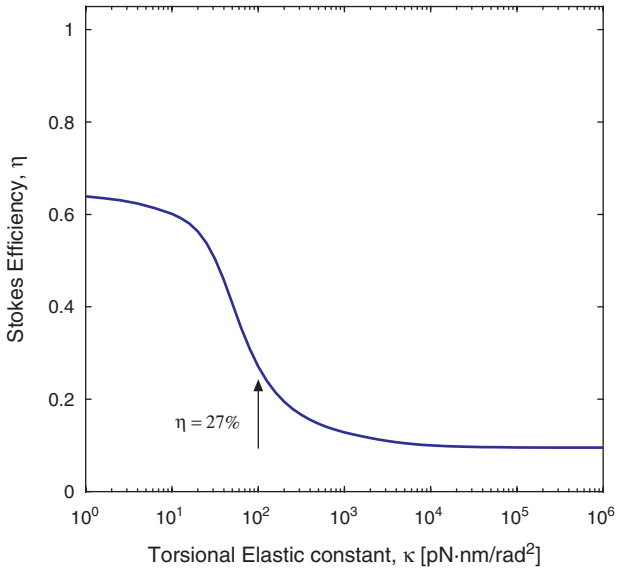

Fig. 4. Stokes efficiency (η) as a function of the torsional elasticity (κ) of the link between the F_1 motor and the actin filament. The results shown are for the case where each 120° rotation is driven by 1 big ratchet step with a free energy change of $\Delta G = 20\ k_B T$. At the estimated torsional elasticity of the link, $\kappa = 100$ pN·nm/rad^2, the Stokes efficiency is only about 27%, far below the observed Stokes efficiency of the F_1ATPase in experiments.[15] Even for a link with torsional elasticity as small as $\kappa = 1$ pN·nm/rad^2, the Stokes efficiency is about 64%, still significantly below the observed Stokes efficiency of the F_1ATPase.

described in the previous section for a wide range of elasticity of the link: from $\kappa = 1$ pN nm/rad^2 to $\kappa = 10^6$ pN nm/rad^2. Figure 4 shows the Stokes efficiency (η) as a function of the coupling elasticity (κ). The Stokes efficiency is obtained by first solving Fokker-Planck Eq. (10) to calculate the actual average velocity of the motor-cargo system and then using formula (16). Figure 4 shows that the Stokes efficiency corresponding to the estimated torsional elastic constant $\kappa = 100$ pN·nm/rad^2 is only about 27%. This result demonstrates that if all of the ATP hydrolysis energy is used to drive one big ratchet step, then the observed high Stokes efficiency of the F_1 ATPase cannot be achieved. This result basically excluded the possibility that hydrolysis of one ATP drives one ratchet step. The conclusion that the F_1 ATPase is not a ratchet has significant implications in the study of the energy transduction of the F_1 ATPase and it is one of several factors that lead us to propose the binding zipper model.[3] The main idea of the binding zipper model is that during the binding transition of ATP from weak binding to strong binding, bonds are formed progressively between the ATP molecule and the surrounding catalytic site. In this process, the binding free energy is utilized uniformly to generate a nearly constant force. At the end of the binding transition, the work is done and the ATP molecule is tightly bound. The hydrolysis step in the ATP cycle is simply to weaken this binding and to divide it into two parts: binding of ADP and binding of Pi. After the hydrolysis, the products are no longer tightly bound so thermal fluctuations can help

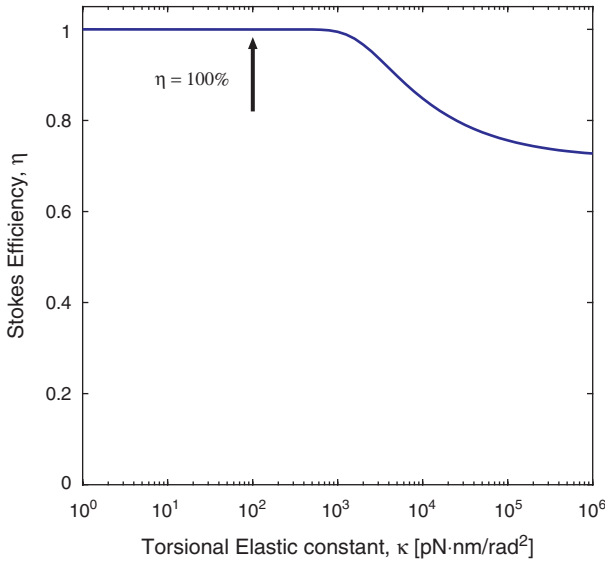

Fig. 5. Stokes efficiency (η) as a function of the torsional elasticity (κ) of the link between the F_1 motor and the actin filament. The results shown are for the case where each 120° rotation is driven by 10 small ratchet steps, each with a free energy change of $\Delta G = 2\ k_B T$. The results clearly demonstrate that by dividing the free energy of one big ratchet step into 10 small ratchet steps, the efficiency is increased dramatically. In particular, notice that even for torsional elasticity as large as $\kappa = 1000$ pN · nm/rad^2, which is 10 times the estimated torsional elasticity of the link, the Stokes efficiency is already very close to 100% if each 120° rotation is driven by 10 small ratchet steps instead of one big ratchet step.

dislodge them from the catalytic site.[3] The release of ADP and Pi is also rectified by the entropy increase after their release. To demonstrate the advantage of utilizing the binding free energy uniformly, we replace the big ratchet step in the example above with 10 small ratchet steps with one tenth of the step size and one tenth of the free energy barrier. More specifically, we use $L = \frac{2\pi}{30} = 12°$ and $\Delta G = 2k_B T$ in (15). We may think one small ratchet step as one tenth of the ATP binding transition process or equivalently the ATP binding transition process consists of 10 small ratchet steps. Figure 5 shows the Stokes efficiency as a function of the coupling elasticity for the case where each $2\pi/3$ rotation of the F_1 motor consists of 10 ratchet steps. In this case, the Stokes efficiency approaches 100% even for values of κ as large as 1000 pN · nm/rad^2. The result demonstrates that when each $2\pi/3$ rotation of the F_1 motor is driven by many small steps (corresponding to the progressive formation of bonds between the ATP molecule and the surrounding catalytic site), the particular form of the driving force for each small step does not affect the Stokes efficiency. This is because the 'lubrication' effect of the elastic coupling and the 'lubrication' effect of thermal fluctuations. Even if each small step is a ratchet where the driving force is an impulse function, the estimated torsional elasticity of the coupling ($\kappa = 100$ pN · nm/rad^2) is more than capable of smoothing it so that the driving force appears as a constant force as measured outside of the motor.

Comparing the results in Figures 4 and 5 (1 ratchet step per $2\pi/3$ rotation versus 10 small ratchet steps per $2\pi/3$ rotation), we observe that elastic coupling is very effective in smoothing the driving force when the motor is driven with many small steps. There are two reasons for this. (a) The larger the number of small steps per $2\pi/3$ rotation, the smaller each sub-step size. For a fixed value of elasticity, it is easier to stretch the elastic link to accommodate a smaller sub-step. (b) The larger the number of steps per $2\pi/3$ rotation, the smaller the amount of free energy consumed per sub-step. When the free energy change involved in each sub-step is comparable to thermal energy ($k_B T$) or smaller, thermal fluctuations will provide a very effective 'lubrication' in addition to the 'lubrication' provided by the elastic coupling.[53]

In summary, we have developed a robust mathematical/numerical formulation for simulating elastically coupled motor-cargo systems. In the formulation, the degree of freedom associated with the relative distance between the motor and the cargo is separated from the degree of freedom associated with the motion of the motor-cargo complex. As a result, very different numerical grids can be adopted for these two degrees of freedom. In this way, the formulation is capable of accommodating a wide range of elasticity. In particular, the stiff spring limit is no longer a numerical difficulty.

Acknowledgments: The author thanks George Oster and Tim Elston for helpful discussions. This work was partially supported by NSF.

References

1. H. C. Berg, Random walks in biology, Princeton, Princeton University Press, NJ **(1993)**, p. 152.
2. H. Wang and G. Oster, *Nature* 396, 279 **(1998)**.
3. G. Oster and H. Wang, *Biochimica et Biophysica Acta (Bioenergetics)* 1458, 482 **(2000)**.
4. C. S. Peskin, G. M. Odell, and G. Oster, *Biophys. J.* 65, 316 **(1993)**.
5. T. Elston, H. Wang, and G. Oster, *Nature* 391, 510 **(1998)**.
6. A. Mogilner and G. Oster, *Eur. J. Biophys.* 28, 235 **(1999)**.
7. R. Astumian, *Science* 276, 917 **(1997)**.
8. P. Reimann, *Physics Reports* 361, 57 **(2002)**.
9. R. D. Astumian and I. Derenyi, *Eur Biophys J.* 27, 474 **(1998)**.
10. E. A. Abbondanzieri et al., *Nature* 438, 460 **(2005)**.
11. A. J. Hunt, F. Gittes, and J. Howard, *Biophys. J.* 67, 766 **(1994)**.
12. M. J. Schnitzer and S. M. Block, *Nature* 388, 386 **(1997)**.
13. H. Itoh et al., *Nature* 427, 465 **(2004)**.
14. Y. Hirono-Hara et al., *Proc. Natl. Acad. Sci. USA*, 120, 4288 **(2005)**.
15. R. Yasuda et al., *Cell* 93, 1117 **(1998)**.
16. K. Visscher, M. Schnitzer, and S. Block, *Nature* 400, 184 **(1999)**.
17. Y. Sambongi et al., *Science* 286, 1722 **(1999)**.
18. S. M. Block et al., *Proc. Natl. Acad. Sci. USA* 100, 2351 **(2003)**.
19. A. Samuel and H. Berg, *Proc. Natl. Acad. Sci.* 92, 3502 **(1995)**.
20. J. Fricks, H. Wang, and T. Elston, *J. Theo. Biol.* 239, 33 **(2006)**.
21. T. Elston, D. You, and C. Peskin, *SIAM J. Appl. Math.* 61, 776 **(2000)**.
22. T. Elston and C. Peskin, *SIAM J. Appl. Math.* 60, 842 **(2000)**.
23. H. Wang and G. Oster, *Europhys. Lett.* 57, 134 **(2002)**.

24. J. Abrahams et al., *Nature* 370, 621 **(1994)**.
25. D. Sabbert, S. Engelbrecht, and W. Junge, *Nature* 381, 623 **(1996)**.
26. H. Noji et al., *Nature* 386, 299 **(1997)**.
27. R. I. Menz, J. E. Walker, and A. G. Leslie, *Cell* 106, 331 **(2001)**.
28. S. M. Block and H. C. Berg, *Nature* 309, 470 **(1984)**.
29. H. C. Berg, *Annu. Rev. Biochem.* 72, 19 **(2003)**.
30. R. Vale, *TIBS* 11, 464 **(1986)**.
31. J. Howard, A. J. Hudspeth, and R. D. Vale, *Nature* 342, 154 **(1989)**.
32. C. Coppin et al., *Proc. Natl. Acad. Sci. USA* 94, 8539 **(1997)**.
33. J. Prost et al., *Phys. Rev. Lett.* 72, 2652 **(1994)**.
34. F. Julicher, A. Ajdari, and J. Prost, *Rev. Modern Phys.* 69, 1269 **(1997)**.
35. S. R. de Groot and P. Mazur, Non-Equilibrium Thermodynamics, Dover, New York **(1984)**.
36. R. Kubo, M. Toda, and N. Hashitsume, Statistical Physics II, Springer, Berlin **(1995)**.
37. F. Reif, Fundamentals of Statistical and Thermal Physics, McGraw Hill, New York **(1965)**.
38. H. Wang, *IEE Proceedings Nanobiotechnology* 150, 127 **(2003)**.
39. P. Boyer, *Biochim. Biophys. Acta* 1140, 2150 **(1993)**.
40. J. Weber and A. E. Senior, *Biochim. Biophys. Acta* 1319, 19 **(1997)**.
41. P. Boyer, *Annu. Rev. Biochem.* 66, 717 **(1997)**.
42. H. Risken, The Fokker-Planck Equation, 2nd edn., Springer-Verlag, New York **(1989)**.
43. C. Gardiner, Handbook of Stochastic Methods, 2nd edn. Springer-Verlag, New York **(1985)**.
44. C. S. Peskin, G. B. Ermentrout, and G. F. Oster, Mechanochemical coupling in ATPase motors, In interplay of genetic and physical porcesses in the development of biological form, Les Houches, Springer-Verlag **(1994)**.
45. C. Doering,, W. Horsthemke, and J. Riordan, *Phys. Rev. Lett.* 72, 2984 **(1994)**.
46. P. Dimroth et al., *Proc. Natl. Acad. Sci. USA* 96, 4924 **(1999)**.
47. G. Oster and H. Wang, *Trends in Cell Biology* 13, 114 **(2003)**.
48. R. Yasuda et al., *Nature* 410, 898 **(2001)**.
49. H. Wang, C. Peskin, and T. Elston, *J. Theo. Biol.* 221, 491 **(2003)**.
50. H. Wang, *Internat. J. Numer. Analy. Modeling*, **(2006)**, In Press.
51. D. Cherepanov, A. Mulkidjanian, and W. Junge, *FEBS Lett.* 449, 1 **(1999)**.
52. Y. Tsuda et al., *PNAS* 93, 12937 **(1996)**..
53. C. R. Doering, *Nuovo Cimento D* 17, 685 **(1995)**.

Received: 1 March 2006. Accepted: 27 March 2006.